

Accepted for Ap.J.

Analysis of a Very Massive DA White Dwarf via the Trigonometric Parallax and Spectroscopic Methods

Conard C. Dahn

US Naval Observatory, Flagstaff Station, P.O. Box 1149, Flagstaff, AZ 86002-1149

`dahn@nofs.navy.mil`

P. Bergeron

*Département de Physique, Université de Montréal, C.P. 6128, Succ. Centre-Ville,
Montréal, Québec, Canada H3C 3J7*

`bergeron@astro.umontreal.ca`

James Liebert

Steward Observatory, University of Arizona, Tucson AZ 85726

`liebert@as.arizona.edu`

Hugh C. Harris

US Naval Observatory, Flagstaff Station, P.O. Box 1149, Flagstaff, AZ 86002-1149

`hch@nofs.navy.mil`

and

S. K. Leggett

UKIRT, Joint Astronomy Centre, 660 North A'ohoku Place, Hilo, HI 96720

`s.leggett@jach.hawaii.edu`

ABSTRACT

By two different methods, we show that LHS 4033 is an extremely massive white dwarf near its likely upper mass limit for destruction by unstable electron

captures. From the accurate trigonometric parallax reported herein, the effective temperature ($T_{\text{eff}} = 10,900$ K) and the stellar radius ($R = 0.00368 R_{\odot}$) are directly determined from the broad-band spectral energy distribution — the parallax method. The effective temperature and surface gravity are also estimated independently from the simultaneous fitting of the observed Balmer line profiles with those predicted from pure-hydrogen model atmospheres — the spectroscopic method ($T_{\text{eff}} = 10,760$ K, $\log g = 9.46$). The mass of LHS 4033 is then inferred from theoretical mass-radius relations appropriate for white dwarfs. The parallax method yields a mass estimate of $1.310\text{--}1.330 M_{\odot}$, for interior compositions ranging from pure magnesium to pure carbon, respectively, while the spectroscopic method yields an estimate of $1.318\text{--}1.335 M_{\odot}$ for the same core compositions. This star is the most massive white dwarf for which a robust comparison of the two techniques has been made.

Subject headings: stars: fundamental parameters — stars: individual (LHS 4033) — white dwarfs

1. INTRODUCTION

LHS 4033 (WD 2349–031) is a white dwarf discussed in a recent paper by Salim et al. (2004). The star has also been part of the Luyten Half Second (LHS) survey $\mu \geq 0.6'' \text{ yr}^{-1}$ white dwarf sample of C. C. Dahn, H. C. Harris, S. K. Leggett, & J. Liebert (2004, in preparation), virtually all of which have been targeted for accurate trigonometric parallaxes at the U.S. Naval Observatory, for purposes of estimating the luminosity function of cool white dwarfs.

In the H-R diagram, this object lies to the left of the diagonal sequence of white dwarfs, indicating that its mass is larger and its radius is smaller than normal. In this paper we show that its mass is, indeed, extraordinarily large for a white dwarf. A few other stars of mass similar to the value we present in this paper for LHS 4033 have been found — i.e. the low-field magnetic star PG 1658+441 (Schmidt et al. 1992; Dupuis et al. 2003, $M \sim 1.31 M_{\odot}$), and the highly-magnetic white dwarf RE J0317–853 (Barstow et al. 1995; Ferrario et al. 1997, $M = 1.35 M_{\odot}$). Note that the application of the Balmer line fitting procedure to these two magnetic stars of high mass is impossible for a ~ 300 MG magnetic white dwarf like RE J0317–853, and the mass of this star has been determined indirectly from the companion. Also, the modelling of the Zeeman triplet components of PG 1658+441 by Schmidt et al. (1992) is only approximate, and it is inherently less accurate due, among other things, to the lack of a rigorous theory of Stark broadening in the presence of the 3.5 MG field. Hence,

both mass estimates are quite uncertain.

Since the spectral type of LHS 4033 is DA and non-magnetic, the mass may be estimated by fits to the Balmer lines (see, e.g., Bergeron et al. 1992) in a much more rigorous fashion. The surface gravity used with suitable evolutionary models yields independent determinations of the mass and radius. The effective temperature may also be estimated from broad-band photometry once the dominant atmospheric constituent is known. This, along with an accurate trigonometric parallax, permits a different estimate of the luminosity, radius, and mass (Bergeron et al. 2001). While it has been possible to compare the parameter determinations of these methods for limited samples of white dwarfs, it is particularly interesting to do so for a massive star.

2. OBSERVATIONAL DATA

Photometry with *BVI* filters was obtained three times with the USNO 1.0 m telescope generally during 1997-1998. *JHK* data were obtained on 1998 October 12 using the IRACAM camera outfitted with the UKIRT system filters and calibrated using UKIRT standards (Hawarden et al. 2001). Colors are reduced to the Johnson system for *B-V*, the Cousins system for *V-I*, and the CIT system for *J-H* and *H-K*. Errors are 0.02 mag in *BVI* and 0.05 in *JHK*. Our optical and infrared photometry for LHS 4033 is given in Table 1. Salim et al. (2004) also report CCD photometry for LHS 4033, on the Johnson-Cousins system, from the Lick Observatory 1 m Nickel telescope. They obtain $B = 17.162 \pm 0.020$, $V = 16.992 \pm 0.017$, $R = 16.987 \pm 0.030$, and $I = 16.936 \pm 0.036$, based on 2-3 observations per band. The corresponding color indices, $B-V = 0.17$ and $V-I = 0.056$, thus agree with our measurements within the uncertainties. In the model atmosphere analysis presented below, we rely on our own photometric measurements only.

Trigonometric parallax observations were carried out over a 6.05 year interval (1997.76 – 2003.81) using the USNO 1.55 m Strand Astrometric Reflector equipped with a Tek2K CCD camera (Dahn 1997). The absolute trigonometric parallax and the relative proper motion and position angle derived from the 150 acceptable frames are given in Table 1. The parallax and apparent V magnitude then yield an absolute magnitude, also included in Table 1. Further details regarding the astrometry for LHS 4033 will appear in a paper on white dwarf parallaxes (Dahn et al. 2004, in preparation).

Finally, optical spectroscopy was secured on 2003 October 1 using the Steward Observatory 2.3-m reflector telescope equipped with the Boller & Chivens spectrograph and a UV-flooded Texas Instrument CCD detector. The 4.5 arcsec slit together with the 600 lines

mm^{-1} grating blazed at 3568 Å in first order provided a spectral coverage of 3120–5330 Å at an intermediate resolution of ~ 6 Å FWHM. The 3000 s integration yielded a signal-to-noise ratio around 55 in the continuum. Our optical spectrum for LHS 4033 is contrasted in Figure 1 with that of G61–17, a DA white dwarf with an effective temperature comparable to that of LHS 4033, but with a normal surface gravity and mass ($T_{\text{eff}} = 10,680$ K, $\log g = 8.06$, $M = 0.64 M_{\odot}$) according to the spectroscopic analysis of the DA stars from the PG sample by J. Liebert, P., Bergeron, & J. B. Holberg (2003, in preparation). The strong decrement of the high Balmer lines already indicates that LHS 4033 is a massive white dwarf.

3. MODEL ATMOSPHERE ANALYSIS

3.1. Photometric Analysis

We first proceed to fit the optical and infrared photometry using the technique described in Bergeron et al. (1997, 2001). Broadband magnitudes are first converted into observed fluxes using Eq. [1] of Bergeron et al. (1997) with the appropriate zero points. The resulting energy distribution is then compared with those predicted from our model atmosphere calculations, with the monochromatic fluxes properly averaged over the same filter bandpasses.

Our model atmospheres are hydrogen-line blanketed LTE models, and assume a pure hydrogen composition. Convection is treated within the mixing-length theory, with the $\text{ML2}/\alpha = 0.6$ formulation following the prescription of Bergeron et al. (1995). The calculations of theoretical spectra are described at length in Bergeron et al. (1991b), and include the occupation probability formalism of Hummer & Mihalas (1988). This formalism allows a detailed calculation of the level populations in the presence of perturbations from neighboring particles, and also provides a consistent description of bound-bound and bound-free transitions.

The observed fluxes f_{λ}^m and Eddington model fluxes H_{λ}^m — which depend on T_{eff} and $\log g$ — for a given bandpass m are related by the equation

$$f_{\lambda}^m = 4\pi (R/D)^2 H_{\lambda}^m , \quad (1)$$

where R/D is the ratio of the radius of the star to its distance from Earth. Our fitting technique relies on the nonlinear least-squares method of Levenberg-Marquardt (Press et al. 1986), which is based on a steepest descent method. The value of χ^2 is taken as the sum over all bandpasses of the difference between both sides of Eq. [1], properly weighted by

the corresponding observational uncertainties. Only T_{eff} and the solid angle $\pi (R/D)^2$ are considered free parameters, while the uncertainties are obtained directly from the covariance matrix of the fit.

We first assume $\log g = 8.0$ and determine the effective temperature and the solid angle, which, combined with the distance D obtained from the trigonometric parallax measurement, yields directly the radius of the star R . The latter is then converted into mass using an appropriate mass-radius relation for white dwarf stars. Here we first make use of the mass-radius relation of Hamada & Salpeter (1961) for carbon-core configurations. This relation is preferred to the evolutionary models of Wood (1995) or those of Fontaine et al. (2001), which extend only up to 1.2 and $1.3 M_{\odot}$, respectively. Uncertainties due to finite temperature effects and core composition will be discussed below. In general, the value of $\log g$ obtained from the inferred mass and radius ($g = GM/R^2$) will be different from our initial assumption of $\log g = 8.0$, and the fitting procedure is thus repeated until an internal consistency in $\log g$ is achieved. The parameter uncertainties are obtained by propagating the error of the photometric and trigonometric parallax measurements into the fitting procedure.

Our best fit to the optical *BVI* and infrared *JHK* photometry of LHS 4033 is displayed Figure 2. The monochromatic fluxes from the best fitting model are shown here as well, although the formal fit is performed using only the average fluxes (filled dots). The solution at $T_{\text{eff}} = 10,900 \pm 290$ K and $R = 0.00368 \pm 0.00013 R_{\odot}$ implies a stellar mass of $M = 1.330 \pm 0.004 M_{\odot}$ and a value of $\log g = 9.43 \pm 0.02$. The parameters of both methods are summarized in Table 2. The predicted absolute visual magnitude obtained from the values of T_{eff} and $\log g$ is $M_V = 14.63$, in perfect agreement with the value derived from the parallax given in Table 1.

3.2. Spectroscopic Analysis

The optical spectrum of LHS 4033 is fitted with the same grid of model atmospheres following the procedure described in Bergeron et al. (1992) and Bergeron et al. (1995). The spectrum is first fitted with several pseudo-Gaussian profiles (Saffer et al. 1988) using the nonlinear least-squares method of Levenberg-Marquardt described above. Normal points defined by this smooth function are then used to normalize the line flux to a continuum set to unity at a fixed distance from the line center. The comparison with model spectra, which are convolved with the appropriate Gaussian 6 Å instrumental profile, is then carried out in terms of these normalized line profiles only. Our minimization technique again relies on the Levenberg-Marquardt method using the H β to H8 line profiles. Our best fit is displayed in Figure 3.

Remarkably, our spectroscopic solution $T_{\text{eff}} = 10,760 \pm 150$ K and $\log g = 9.46 \pm 0.04$, which translates into $M = 1.335 \pm 0.011$ and $R = 0.00358 \pm 0.00019 M_{\odot}$ using the Hamada-Salpeter mass-radius relation for carbon-core configurations, is in excellent agreement with the solution obtained with the photometry and trigonometric parallax method. This is arguably the most massive white dwarf subjected to a rigorous mass determination (see, e.g., Table 3 of Dupuis et al. 2002). Note that despite the extreme surface gravity of LHS 4033, the Hummer-Mihalas formalism used in the line profile calculations remains perfectly valid, since the density at the photosphere remains low ($\rho \sim 10^{-5}$ g cm⁻³) as a result of the high opacity of hydrogen at these temperatures.

3.3. Mass-Radius Relation

In a venerable paper, Hamada & Salpeter (1961) first employed an equation-of-state (EOS) including coulomb “corrections” to the pressure and energy of a degenerate Fermi gas (Salpeter 1961) to calculate the mass-radius-central density relations for models composed of helium through iron. These corrections to the classic Chandrasekhar EOS for degenerate matter are more important at high mass. It may also be noted that, especially at the relatively low effective temperature of LHS 4033, neglect of the internal energy of the ions (“zero-temperature” modelling) is likely to be a reasonable assumption.

Since LHS 4033 may have a core composed of material much heavier than carbon, we must explore the effects of core composition on the results of our analysis. We compare in Figure 4 the mass-radius relation obtained from the detailed evolutionary carbon- and carbon/oxygen-core models of Fontaine et al. (2001, see also Bergeron et al. 2001) with the Hamada-Salpeter zero-temperature configurations for carbon and magnesium at a mass of $1.3 M_{\odot}$, the highest mass of the Fontaine et al. models. At the effective temperature and mass of LHS 4033, the carbon- or carbon/oxygen-core models of Fontaine et al. reveal that finite temperature effects are extremely small, and account for an increase in radius of only $\sim 0.5\%$ (i.e. by comparing the radius at 10,000 K with the value at 3500 K where it becomes constant). Moreover, at the temperature of LHS 4033, the carbon-core models of Fontaine et al. and Hamada-Salpeter differ by only 2.7 % in radius, or $0.007 M_{\odot}$ in mass. Details of the equation-of-state are thus also negligible in the present context. Finally, the Mg and C configurations of Hamada-Salpeter differ by 7.4 % in radius, or $0.02 M_{\odot}$ in mass. Indeed, the parallax method with the Mg configurations yields a mass of $1.310 M_{\odot}$ (instead of $1.330 M_{\odot}$ when C configurations are used), while the spectroscopic method yields a mass of $1.318 M_{\odot}$ (instead of $1.335 M_{\odot}$). These results are also reported in Table 2. We thus argue that our mass estimates are uncertain by $0.02 M_{\odot}$ at the most.

4. DISCUSSION

The theoretical prediction is that, with a mass near $1.33 M_{\odot}$, LHS 4033 has been through carbon burning, *if* it has evolved as a single star. Perhaps more plausible is the possibility that massive white dwarfs apart from those found in young clusters or associations are generally the results of mergers of more ordinary, probably C-O white dwarfs (cf. Bergeron et al. 1991a; Vennes et al. 1996; Marsh et al. 1997). In the former case, LHS 4033 can be expected to have an interior composed of some mix of O^{16} , Ne^{20} , Mg^{24} and even Na^{23} (an O-Ne-Mg core; Garcia-Berro & Iben 1994; Ritossa et al. 1999, and references therein). For our mass determination of $1.33 - 1.34 M_{\odot}$, the Hamada-Salpeter calculations place LHS 4033 very near their predicted maximum mass of $1.363 M_{\odot}$ for Mg^{24} and $1.396 M_{\odot}$ for C (with other species with atomic weights intermediate between these extremes having values presumably in between). Thus, there is little difference between the assumptions of an O-Ne-Mg interior (an unusual single star), and that of a normal C-O composition (binary origin). Above this mass limit – significantly less than that of Chandrasekhar near $1.4 M_{\odot}$ – electron captures (traditionally called inverse beta decays) will produce increasingly neutron-rich nuclei, increasing the mean molecular weight per particle, and resulting in some kind of detonation of the core (see, e.g., Arnett 1996).

The high mass and small radius cause the gravitational redshift of LHS 4033 to be much larger than for a normal white dwarf: $v_{GR} = 0.635 (M/M_{\odot}) (R_{\odot}/R) = 237 \text{ km s}^{-1}$. This fact accounts for the high radial velocity (206 km s^{-1}) observed by Salim et al. (2004) without requiring that the star have a high space velocity. The tangential velocity, using the proper motion and distance reported in Table 1, is 97 km s^{-1} , and also is not as large as would be derived from a photometric distance estimate assuming the star had a normal gravity. The components of its space velocity, based on the proper motion in Table 1 and the radial velocity observed by Salim et al. corrected for the gravitational redshift above, are $(U, V, W) = (87, -11, 31) \text{ km s}^{-1}$. (These values have been corrected for the Sun's peculiar velocity, and U is away from the Galactic center and V is in the direction of Galactic rotation.) This space velocity is consistent with the kinematics of the Galaxy's old disk.

We thank S. Boudreault for the reduction of the optical spectrum, and G. Fontaine for useful discussions. The astrometric observations were carried out as part of the USNO parallax program, and we thank the following individuals who contributed some of the frames used here – Blaise Canzian, Harry Guetter, Stephen Levine, Chris Luginbuhl, Alice Monet, Dave Monet, Ron Stone, and Dick Walker. This work was supported in part by the NSERC Canada and by the Fund FQRNT (Québec). JL acknowledges support from the National Science Foundation through grant AST-0307321 for study of white dwarfs. UKIRT, the

United Kingdom Infrared Telescope, is operated by the Joint Astronomy Centre on behalf of the U.K. Particle Physics and Astronomy Research Council.

REFERENCES

Arnett, D. 1996, in *Supernovae and Nucleosynthesis* (Princeton: Princeton University Press), 168

Barstow, M. A., Jordan, S., O'Donoghue, D., Burleigh, M. R., Napiwotzki, R., & Harrop-Allin, M. K. 1995, *MNRAS*, 277, 971

Bergeron, P., Kidder, K. M., Holberg, J. B., Liebert, J., Wesemael, F., & Saffer, R. A. 1991a, *ApJ*, 372, 267

Bergeron, P., Leggett, S. K., & Ruiz, M. T. 2001, *ApJS*, 133, 413

Bergeron, P., Ruiz, M. T., & Leggett, S. K. 1997, *ApJS*, 108, 339

Bergeron, P., Saffer, R. A., & Liebert, J. 1992, *ApJ*, 394, 228

Bergeron, P., Wesemael, F., & Fontaine, G. 1991b, *ApJ*, 367, 253

Bergeron, P., Wesemael, F., Lamontagne, R., Fontaine, G., Saffer, R. A., & Allard, N. F. 1995, *ApJ*, 449, 258

Dahn, C.C. 1997, in *Fundamental Stellar Properties: The Interaction between Observations and Theory*, IAU Symp. No. 189, ed. T.R. Bedding, A.J. Booth, & J. Davis (Dordrecht: Kluwer), 19

Dupuis, J., Chayer, P., Vennes, S., Allard, N.F., & Hébrard, G. 2003, *ApJ*, 598, 486

Dupuis, J., Vennes, S., & Chayer, P. 2002, *ApJ*, 580, 1091

Ferrario, L., Vennes, S., Wickramasinghe, D. T., Bailey, J. A. & Christian, D.J. 1997, *MNRAS*, 292, 205

Fontaine, G., Brassard, P., & Bergeron, P. 2001, *PASP*, 113, 409

Garcia-Berro, E. & Iben, I. Jr. 1994, *ApJ*, 434, 306

Hamada, T., & Salpeter, E. E. 1961, *ApJ*, 134, 683

Hawarden, T. G., Leggett, S. K., Letawsky, M. B., Ballantyne, D. R., & Casali, M. M. 2001, *MNRAS*, 325, 563

Hummer, D. G., & Mihalas, D. 1988, *ApJ*, 331, 794

Marsh, M. C., Barstow, M. A., Buckley, D.A., Burleigh, M. R., Holberg, J. B., Koester, D., O'Donoghue, D., Penny, A. J., & Sansom, A.E. 1997, MNRAS, 286, 369

Press, W. H., Flannery, B. P., Teukolsky, S. A., & Vetterling, W. T. 1986, Numerical Recipes (Cambridge: Cambridge University Press)

Ritossa, C., Garcia-Berro, E., & Iben, I. Jr. 1999, ApJ, 515, 381

Saffer, R. A., Liebert, J., & Olszewski, E. W. 1988, ApJ, 334, 947

Salim, S., Rich, R. M., Hansen, B. M., Koopmans, L. V. E., Oppenheimer, B. R., & Blandford, R. D. 2004, ApJ, in press

Salpeter, E. E. 1961, ApJ, 134, 669

Schmidt, G. D., Bergeron, P., Liebert, J., & Saffer, R. A. 1992, ApJ, 394, 603

Vennes, S., Thejll, P. A., Wickramasinghe, D. T., & Bessell, M. S. 1996, ApJ, 467, 782

Wood, M. A. 1995, in 9th European Workshop on White Dwarfs, NATO ASI Series, ed. D. Koester & K. Werner (Berlin: Springer), 41

Table 1. Photometric and Astrometric Data for LHS 4033

Parameter	Value
V	16.98 ± 0.02
$B-V$	$+0.19 \pm 0.03$
$V-I$	$+0.07 \pm 0.03$
J	16.97 ± 0.05
$J-H$	$+0.05 \pm 0.07$
$H-K$	-0.10 ± 0.07
π_{abs} (mas)	33.9 ± 0.6
μ_{rel} (mas yr $^{-1}$)	701.4 ± 0.2
PA (deg)	66.3 ± 0.1
Distance (pc)	29.5 ± 0.5
M_V	14.63 ± 0.04

Table 2. Atmospheric Parameters of LHS 4033

Core	Method	T_{eff} (K)	$\log g$	R/R_{\odot}	M/M_{\odot}
C	Parallax	$10,900 \pm 290$	9.43 ± 0.02	0.00368 ± 0.00013	1.330 ± 0.004
	Spectroscopy	$10,760 \pm 150$	9.46 ± 0.04	0.00358 ± 0.00019	1.335 ± 0.011
Mg	Parallax	$10,900 \pm 290$	9.42 ± 0.02	0.00368 ± 0.00013	1.310 ± 0.004
	Spectroscopy	$10,760 \pm 150$	9.46 ± 0.04	0.00355 ± 0.00019	1.318 ± 0.011

Fig. 1.— Comparison of the optical spectrum of LHS 4033 with that of G61–17, a white dwarf with comparable effective temperature ($T_{\text{eff}} = 10,680$ K) but with a normal mass of $M = 0.64 M_{\odot}$ ($\log g = 8.06$). The spectra are normalized at 4400 Å and are shifted vertically by 0.5 for clarity.

Fig. 2.— Fits to the energy distribution of LHS 4033 with pure hydrogen models. The optical *BVI* and infrared *JHK* photometric observations are shown by the error bars. The solid line corresponds to the model monochromatic fluxes, while the filled circles represent the average over the filter bandpasses (including the model prediction at R).

Fig. 3.— Model fits to the individual Balmer line profiles of LHS 4033. All lines are normalized to a continuum set to unity and offset vertically from each other by a factor of 0.2. Values of T_{eff} and $\log g$ have been determined from $\text{ML2}/\alpha = 0.6$ models, while the stellar mass has been derived from the mass-radius relation of Hamada & Salpeter (1961) for carbon-core configurations.

Fig. 4.— Comparison of the mass-radius relation at $M = 1.3 M_{\odot}$ obtained from the evolutionary carbon- and carbon/oxygen-core models of Fontaine et al. (2001, FBB/C and FBB/C-O, respectively) and the carbon and magnesium zero-temperature configurations of Hamada & Salpeter (1961, HS/C and HS/Mg, respectively).

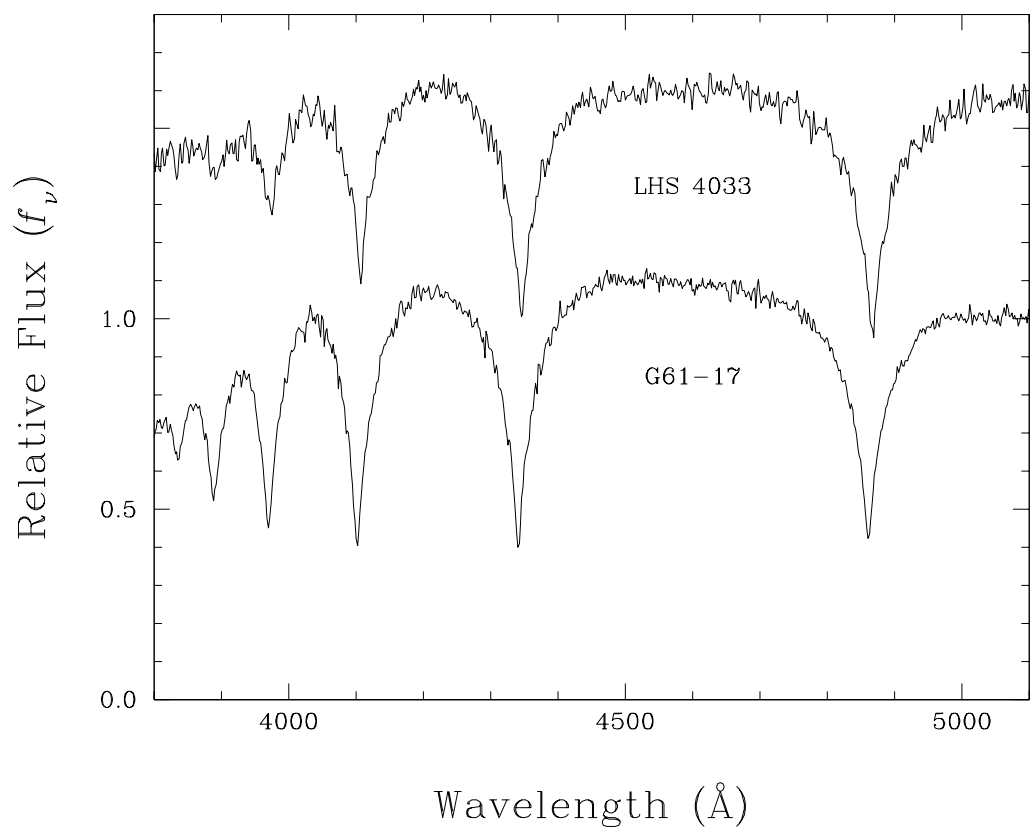


Figure 1

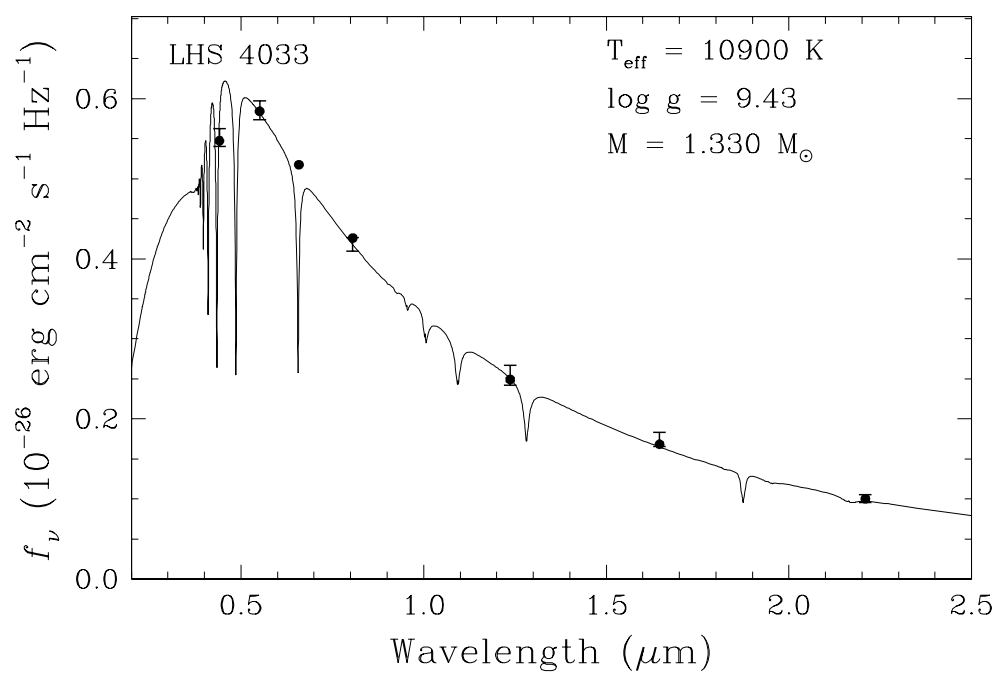


Figure 2

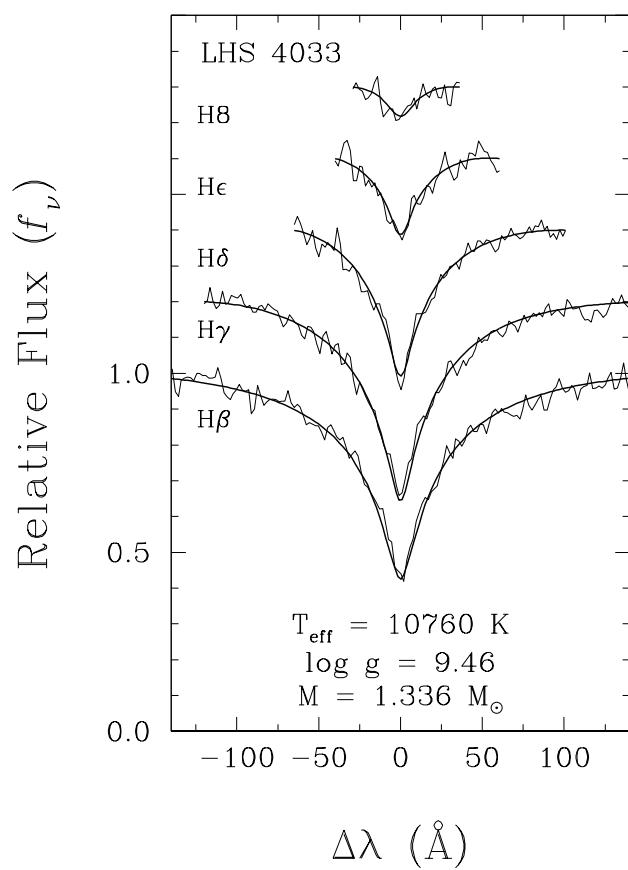


Figure 3

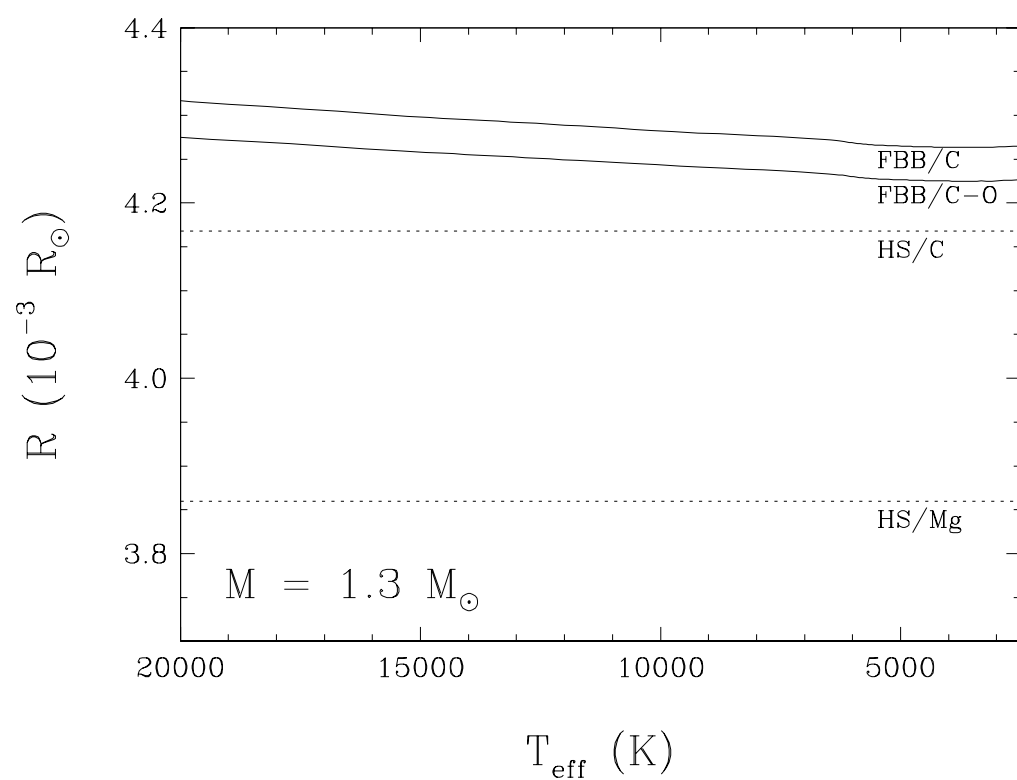


Figure 4